Catalysis Communications 175 (2023) 106612

Contents lists available at ScienceDirect

Catalysis Communications

journal homepage: www.elsevier.com/locate/catcom

Al- and Mg-doped $SrTiO_3$ perovskite steps: The catalytic performance for oxidative coupling of methane

Silvia Carlotto [a,b,*]

[a] Department of Chemical Sciences, University of Padova, via F. Marzolo 1, 35131 Padova, Italy
[b] Institute of Condensed Matter Chemistry and Technologies for Energy (ICMATE), National Research Council (CNR), c/o Department of Chemical Sciences, University of Padova, via F. Marzolo 1, 35131 Padova, Italy

ARTICLE INFO

Keywords:
OCM reaction
Step defectivity
Al- and Mg-doped perovskites
DFT periodic calculations

ABSTRACT

One of the most important processes for converting methane into value-added chemical products is the reaction of the oxidative coupling of methane. The catalytic performance of a heterogenous catalyst can be evaluated using the first principles. The simultaneous presence of defects (oxygen vacancies, metal dopants and edges) on perovskites makes the simulations more realistic and closer to the experimental conditions. Results showed that CH_3 adsorption and formation energy of the oxygen vacancy are sufficient to verify catalytic activity. The comparison of the steps and the surface simulations shows different properties and that the step is not always the preferred catalytic site.

1. Introduction

In industrial manufacturing, where natural gas is the raw material, the conversion of methane into value-added chemical products is a desirable process that will play an increasing role in the future [1]. The major interest is in a process called oxidative coupling of methane (OCM), in which the catalysed reaction of methane in the presence of oxygen produces ethane and ethylene. In this reaction, CH_4 is adsorbed onto a metal oxide surface in order to produce a CH_3 radical that will be released in the gas phase to form olefines [2]. Since the pioneering work of Keller and Bhasin in 1982 [3], a great deal of research has been conducted on the OCM reaction, and current developments include the chemistry of methane activation [4,5], the use of alternative oxidants [6], reactor technologies [7–9], thermodynamic limitations [10], and heterogeneous catalytic methane conversion [11–13]. Focusing on the more proper chemical aspects, recent advances concern the active site, acid-base properties, oxygen vacancy, and surface reducibility, as well as discussed in excellent reviews [5,12].

In the OCM reaction, one of the most intriguing challenges concerns the first part of the activation mechanism involving the C—H bond breaking. Indeed, to fully understand the mechanism, experimental [2,14] and computational [15,16] studies have focused on this aspect. Therefore, the development of the best performing and commercially viable catalyst that can facilitate this breaking is the goal of the researcher's efforts. Catalytic performance must be evaluated through a set of parameters to drive the synthesis of new materials. These parameters quantify the selectivity and yield of the heterogeneous catalyst. They can be directly related to structural and chemical properties. It is generally accepted in the literature that the catalytic activity in the OCM reaction can be described using three different parameters: (i) activity is related to the ability to break the C—H bond; (ii) selectivity to CH_3 adsorption strength and (iii) surface reducibility is related to the ability to form stable oxygen vacancies [17–22]. All these values can be obtained computationally and associated with the structure of the catalyst.

Several classes of materials have been tested as heterogeneous catalysts for the OCM process. Metal oxide surfaces, for example, have been extensively studied both experimentally [23–26] and theoretically [17,21,27,28]. Among them, the perovskites (general formula ABO_3) are capable of readily adsorbing hydrogen [29], which plays a critical role in the C—H activation mechanism, and show a good capability to form stable oxygen vacancies [17,27,30–34]. Both these properties are crucial in oxidative coupling reactions, as reported by Fung et al.as reported by Fung et al. [20]. Using first principles, they studied the role of dopants at sites A and B on the C—H activation energy and suggested a correlation between the oxygen surface reactivity and the C—H activation energy, although a general trend was elusive.

Among the free Rare Earth perovskites, catalytic performance has been studied for the OCM reaction [12,21–23]. Bai et al. [35] considered

* Corresponding author.
E-mail address: silvia.carlotto@unipd.it.

https://doi.org/10.1016/j.catcom.2023.106612
Received 20 October 2022; Received in revised form 5 December 2022; Accepted 13 January 2023
Available online 15 January 2023

the impact of $SrTiO_3$ surface composition and found improved performance with Sr surface enrichment. Fakhroueian and co-workers [22] reported an increment in selectivity with Na and Ba doping at sites A and B, while Ivanov et al. [20] showed that different dopants at both A- and B-sites promote catalytic performance and in particular catalyst selectivity. Finally, Lim et al. [21] combined experimental and first-principles calculations on catalyst design for the oxidative coupling of methane and found an optimal range for CH_3 adsorption for $SrTiO_3$ surfaces doped with metals and lanthanides. However, a fundamental understanding of the effects of the dopant on a no-ideal flat $SrTiO_3$ perovskite surface on catalytic reactivity/selectivity for OCM has not yet been achieved.

Therefore, this study aims to evaluate, using first principles, the catalytic performance of pure and doped $SrTiO_3$ in a more realistic system than an ideal flat surface. For this purpose, oxygen vacancies, different metal dopants and an extended structural defectivity as edges and facets are considered by modelling the dopant reduced steps (see Fig. 1). The Mg and Al dopants were considered for both sites A and B. The results demonstrated that the experimental catalytic activity can be explained by using selected calculated parameters, such as the CH_3 adsorption and the oxygen vacancy formation energy, to verify the selectivity/surface activity and reducibility, respectively. A comparison between the step and the surface under similar conditions was also performed, showing that step (i) has different properties than the surface and (ii) is not necessarily the best performing catalytic site. In fact, the stability of vacancy and adsorption properties, while maintaining similar trends, change dramatically from a quantitative point of view. These variations strongly alter the performance of the catalyst and highlight how the results obtained for ideal surfaces are not fully transferable on the step model.

2. Computational details

The Quantum-ESPRESSO software package [36,37] is used to calculate the relaxed structures and the adsorption properties of pure and doped $SrTiO_3$ steps. The computational setup was previously adopted [29,34,38,39] on $SrTiO_3$ steps, where the spin-polarized Kohn–Sham equations are solved with the PBE exchange–correlation functional [40] and core–valence interactions are considered through Vanderbilt ultrasoft pseudopotentials [41]. Ti (3 s and 3p) and Sr (4 s and 4p) semicore states are explicitly treated. A kinetic energy cutoff of 25 Ry, while a 250 Ry cutoff is used for the augmented charge). A 2×2 Monkhorst-Pack mesh is used for the Brillouin zone. For both pure and doped calculations, the lattice constant of pure compound ($a = 3.931$ Å) [31] is used. To avoid interactions, a thick vacuum space of 19 Å is used between the surfaces of the slab. Calculations are performed on a 3×4 $SrTiO_3$ (110) slab (five SrTiO and four O_2 atomic layers for each slab), where the step is obtained by removing SrO units. Only the top three layers of the slab are relaxed, while the other ones are kept fixed.

The oxygen vacancy formation energy $E_f(Vx)$, with x = 1, 2 for a single oxygen vacancy, is calculated as total energy differences between the unreduced slab and the reduced slab plus a half free O_2 molecule from the equation:

$$E_f(Vx) = E[Vx@step] + \frac{1}{2}E[O_2] - E[step]$$

where $E[Vx\ @\ step]$ is the total energy of the step containing the oxygen vacancy, $E[O_2]$ is the energy of the isolated oxygen molecule,

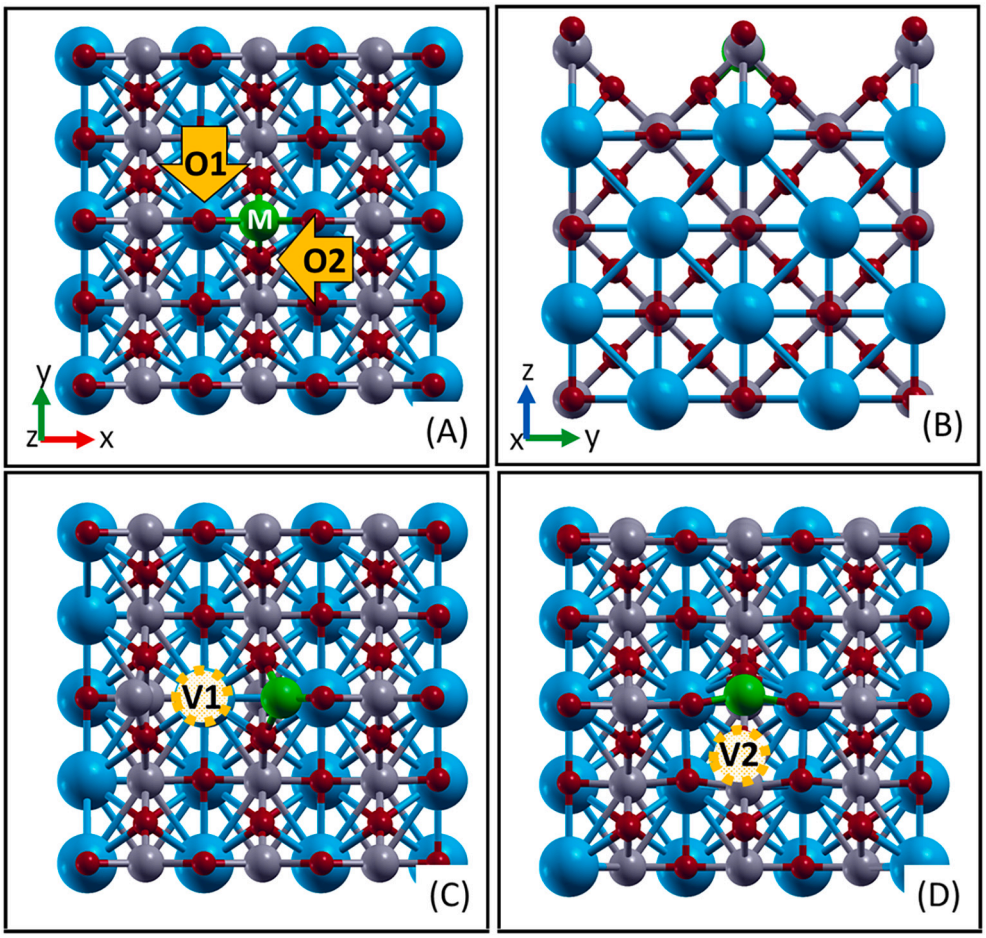

Fig. 1. (A)). Cyan, grey, red and green spheres are Sr, Ti, O and Al atoms, respectively.

and $E[step]$ is the total energy of the oxidized doped/undoped step. A correction was applied to compensate for the DFT-GGA overestimation of the O_2 dissociation energy is applied a correction [28,42].

Similarly, the adsorption energies of the different species (CH_4 and CH_3) are obtained as the difference between the step with one adsorbed molecule $E_{ads}(CH_4, CH_3)$, minus the sum of the bare step $E[step]$ and the isolated molecule energy $E[CH_4, CH_3]$.

$$E_{ads}(CH_4, CH_3) = E[CH_4, CH_3@step] - E[CH_4, CH_3] - E[step]$$

For the $E_{ads}(H)$, the half energy of the isolated H_2 molecule is considered. All isolated species (CH_4, CH_3 radical, H_2 and O_2) are calculated in a $10 \times 10 \times 10$ A^3 cubic box.

3. Results

Various OCM reaction mechanisms have been proposed in the literature, whose common elements are reagents (CH_4 and O_2) and products (hydrocarbons and water) in the presence of a catalyst [17,18,21,43–46], where the type of hydrocarbons depends on the ratio of methane and oxygen. Several authors propose a simplified OCM reaction mechanism [17,45,46] that can be described in five stages.

The OCM process (Scheme 1) can be represented globally as eq. 1:

$$2CH_4 + O_2 \rightarrow C_2H_4 + 2H_2O \quad (1)$$

Both gas-phase and surface reactions play an important role in the formation of desired products. However, in this study, the attention will be focused on the catalytic active sites, thus only on reactions directly involving the heterogeneous catalyst. This choice is justified by the fact that the methane activation stage is generally accepted as the rate-determining step [17,45] and the purpose of the study is to select the optimal heterogeneous catalyst. Thus, all CH_3 radical reactions in the gas phase are outside of the scope of this study.

In presence of a heterogeneous catalyst, the CH_4 adsorption onto the surface oxygen atom (Eq. 2) leads to the CH_3 radical formation (Eq. 3a), which should be released into the gas-phase (Eq. 3b):

$$CH_4 + O_s \rightarrow [CH_4]_s \quad (2)$$

$$[CH_4]_s \rightarrow \bullet [CH_3]_s + H_s \quad (3a)$$

$$\bullet[CH_3]_s \rightarrow \bullet CH_3 \quad (3b)$$

where the subscript s is used to label the surface adsorbed species.

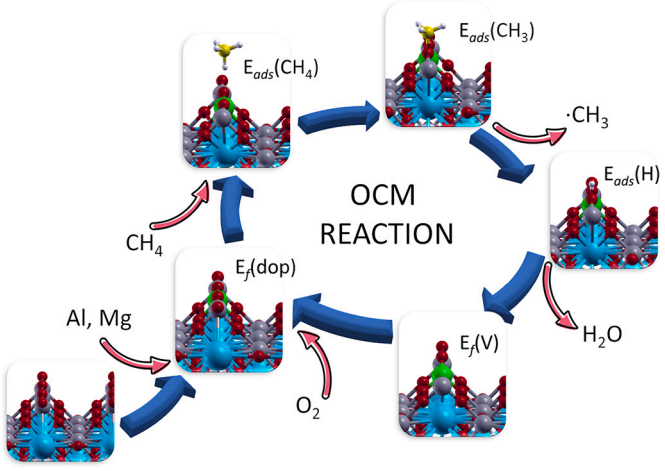

Scheme 1. Schematic diagram for the OCM mechanism stages that involved the surface (see the text for the description of each stage). The stage in Eq. 3b is not shown because it did not involve the heterogenous catalyst (step). Colour code as in Fig. 1. In addition, the yellow and white spheres represent C and H atoms, respectively.

Hydrogen is adsorbed on the oxygen surface. CH_3 radicals in the gas phase react to form C_2H_4. To restore the original catalyst, the adsorbed hydrogens react with surface oxygen to form the water molecule and an oxygen vacancy (Eq. 4)

$$2\,[OH]_s \rightarrow [*]_s + O_s + H_2O \quad (4)$$

where $[*]_s$ is the oxygen vacancy. Molecular oxygen heals this vacancy to obtain the original catalyst again (eq. 5)

$$[*]_s + {}^1\!/_2 O_2 \rightarrow O_s \quad (5)$$

To evaluate the catalytic performance of the catalyst for the OCM reaction (Scheme 1), it is possible to correlate the most relevant stages of the mechanism with some calculable parameters. Specifically:

i) activity depends on the C—H activation process that allows the formation of the CH_3 radical that must desorb in the gas phase to form the desired products. This parameter is obtained from eq. 3a and can be related to the activation value of the C—H bond;
ii) selectivity depends on the ability of the CH_3 radical to adsorb/desorb from the surface. This stage competes with the previous one because any factor that enhances adsorption reduces its performance. This parameter is obtained from eq. 3b and can be related to the value of the CH_3 adsorption energy;
iii) reducibility depends on the ability to form and stabilize oxygen vacancy, and any factor that promotes the formation of the oxygen vacancy increases the performance. This parameter is related to eq. 4, where the adsorbed H atoms were released as water molecules and can be related to the value of the oxygen vacancy formation energy.

3.1. Formation and oxygen vacancy formation energies

When dealing with a doped system, the first thing to be evaluated is the formation energy $E_f(dop)$ of dopant substitutional, which is calculated according to the formula:

$$E_f(dop) = E[dop@step] - E[step] + E[Ti] - E[dop]$$

where $E[dop\ @\ step]$ is the total energy of the supercell containing the dopant (Al or Mg) impurity, $E[step]$ is the total energy of the pure step supercell, while $E[Ti]$ and $E[dop]$ are the energies of Ti and dopant in their stable metallic phases. This yields at B-site 0.79 and 0.35 eV for Al and Mg dopants, respectively, and at the A-site 1.64 eV for the Mg dopant (see Table 1). More positive formation energies indicate less stable defects, so these values suggest that it is easier to insert a dopant at the B-site. Also, a comparison with the flat (100) $SrTiO_3$ surface shows that it is easier to insert a dopant at the B-site of the step than at the surface, where the values for Al- and Mg-doped at the B site are 1.11 eV and 1.54 eV [47]. This behaviour has also been previously observed for other dopants (Co or Cu) [20].

Table 1
Formation energies $E_f(dop)$, oxygen vacancy formation energies $E_f(Vx)$, and CH_3, CH_4, and H adsorption energies for pure, Al- and Mg-doped surfaces. The oxygen vacancy and the adsorption (O1 and O2) sites are labelled in Fig. 1. All energies are given in eV.

	Pure	Al (B-site)	Mg (B-site)	Mg (A-site)
$E_f(dop)$	//	0.79	0.35	1.64
$E_f(V1)$	5.03	3.44	2.16	3.74
$E_f(V2)$	4.38	3.13	0.96	3.01
${}^{O1}E_{ads}(CH_4)$	−0.49	−0.43	−0.37	−1.69
${}^{O2}E_{ads}(CH_4)$	−0.48	//	−0.43	−1.38
${}^{O1}E_{ads}(CH_3)$	−1.60	−2.54	−3.70	−2.81
${}^{O2}E_{ads}(CH_3)$	−1.31	−1.90	−3.50	−2.04
${}^{O1}E_{ads}(H)$	−0.01	−1.06	−2.18	−1.35
${}^{O2}E_{ads}(H)$	−0.08	−0.92	−2.29	−1.47

The inclusion of another defect, a single oxygen vacancy, is more complex than for the flat surface because multiple sites must be considered. Specifically, an oxygen atom is removed from the first or second layer of the slab model. The vacancy sites are labelled as V1 and V2 (see Fig. 1), and the formula for calculating the vacancy formation energy $E_f(Vx)$, with x = 1, 2 is given in computational details.

For the pure step, the values of $E_f(V1)$ and $E_f(V2)$ are 5.03 and 4.38 eV, respectively. Depending on the site, they are slightly higher (V1) or significantly lower (V2) than those previously calculated for the (1 0 0) surface (4.89 eV [47]). Indeed, for both Al and Mg-doped steps at both A and B sites, $E_f(V1)$ and $E_f(V2)$ values are significantly lower than those for the pure step. As also observed for other dopants, impurity promotes the formation of vacancy, particularly at the V2 site. In more detail, for the Al- and Mg-doped systems at the B-site, $E_f(V1)$ and $E_f(V2)$ values (3.44/3.13 eV and 2.16/0.96 eV for Al and Mg at V1/V2 sites respectively) are higher than the values at the doped (1 0 0) surface (2.31 and − 0.09 eV for Al- and Mg-doped, respectively [47]). All values are shown in Table 1.

3.2. The surface selectivity and the surface activity: CH_3 and H adsorption energies

The first stage to consider for surface selectivity and activity is the CH_4 adsorption on the step. In our previous work on the doped $SrTiO_3$ surface, both metal and oxygen adsorption sites were considered, but the former is always disadvantaged compared to the latter [47]. Therefore, only the two oxygen sites closest to the metal were calculated. Fig. 2 shows the O1 and O2 sites on the ridge and side of the step, respectively for the pure step. The $E_{ads}(CH_4)$ energy is calculated as shown in the computational details section.

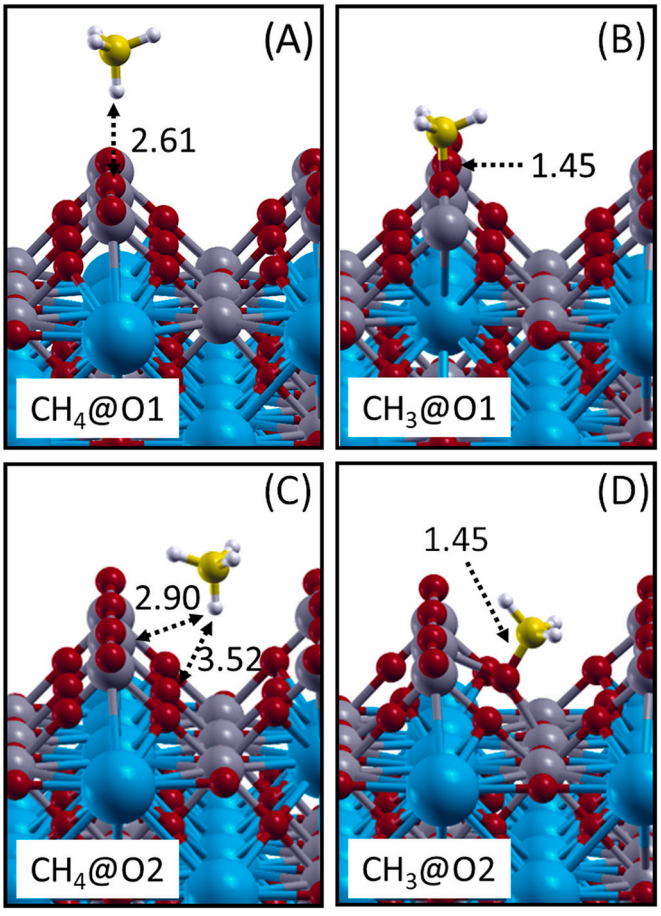

Fig. 2. CH_4 / CH_3 adsorption at O1 (A/B) and O2 (C/D) sites for the pure step. All distances are reported in Å. Colour code as in Fig. 1. In addition, the yellow and white spheres represent C and H atoms, respectively. (For interpretation of the references to colour in this figure legend, the reader is referred to the web version of this article.)

Comparison of the $E_{ads}(CH_4)$ energies of the pure and doped steps at the different adsorption sites shows that (i) for the pure and B-site doped steps, the adsorption energies are similar; (ii) for the A-site doped step, this value is significantly higher than for the other systems; and (iii) there are only slight variations between sites O1 and O2. All values are shown in Table 1. Interestingly, a direct comparison between the surface and steps with pure and Al- and Mg-doped at B-site reveals that the $E_{ads}(CH_4)$ energies at the step are always higher than at the surface. These results prove that in the presence of structural defectivity, the step becomes the preferred adsorption site for CH_4.

The second stage of the OCM mechanism involves the adsorption of CH_3, which is generally recognized as a measure of catalyst selectivity. Actually, after CH_4 adsorption, two competitive processes can occur: (i) CH_3 can be realised at the gas phase and reacts to form the desired value-added chemical products or (ii) it can anchor itself firmly at the step and avoid product formation. A catalyst with good performance has a high capability to release CH_3: selectivity decreases as the CH_3 adsorption energy increases. Similarly to CH_4, the CH_3 adsorption energy is obtained as the difference between the energy of the step with adsorbed CH_3, minus the sum of the energy of the step and the isolated $\cdot CH_3$ radical. The results in Table 1 show lower adsorption values for the pure step, while the doped ones have higher values. In contrast to the trend of CH_4 adsorption, there is a clear difference between the two adsorption sites (O1 and O2) for all systems (see Fig. 3). The lateral site O2 exhibits systematically lower CH_3 adsorption energies than the edge one O1. Comparison of these values with those of the surface shows a common qualitative trend [47]: adsorption energies for pure systems are generally lower than for the doped ones.

After reducibility (oxygen vacancy formation energy) and selectivity (CH_3 adsorption energy), the last characteristic for testing catalytic performance is activity. Three different ways to calculate activity are reported in the literature: (i) the H adsorption energy $E_{ads}(H)$ [18,19]; (ii) the C—H dissociation energy [21]; and (iii) the activation energy [17]. In a preview work on the catalytic properties of $SrTiO_3$ pure and doped surfaces, these methods are commented on by items and the linear dependence of the second and the third on the first is reported and demonstrated [47]. Therefore, attention will be focused only on the first method, in which the $E_{ads}(H)$ is calculated as the difference between the step with adsorbed H and the sum of the bare step and half the energy of the free H_2 molecule.

Calculated results in Table 1 show almost negligible interaction between the H atom and the pure step at both adsorption sites, while the values are sensitively higher (up to 2.29 eV) for the doped steps. In particular, the Al-doped/ Mg-doped steps (B-site) have lower/higher H adsorption energy. For all systems, the energy difference between the H adsorption sites (O1 and O2) is around 0.15 eV. The comparison between pure and doped surfaces with the corresponding steps highlights higher values for the surface systems [47]. A too strong H-catalyst interaction is not a favourable aspect: the adsorbed H must be realised in the gas phase as water to restore the initial catalyst.

4. Discussion

In the preview sections, $E_f(Vx)$, $E_{ads}(H)$, and $E_{ads}(CH_3)$ parameters, which are useful to verify the catalytic performance, are calculated for pure and doped steps. Fig. 4a and b show that linear trends exist between $E_f(Vx)$ and $E_{ads}(CH_3)$ / $E_{ads}(H)$ values for both O1 and O2 adsorption sites and for both V1 and V2 vacancy sites. These correlations are very similar to those found in pure and doped surfaces, which means that the step defect can alter the absolute values but not the overall trends of these parameters. Since there is a linear correlation between $E_{ads}(CH_3)$ / $E_{ads}(H)$ values, only one can be considered. The literature [21,47]

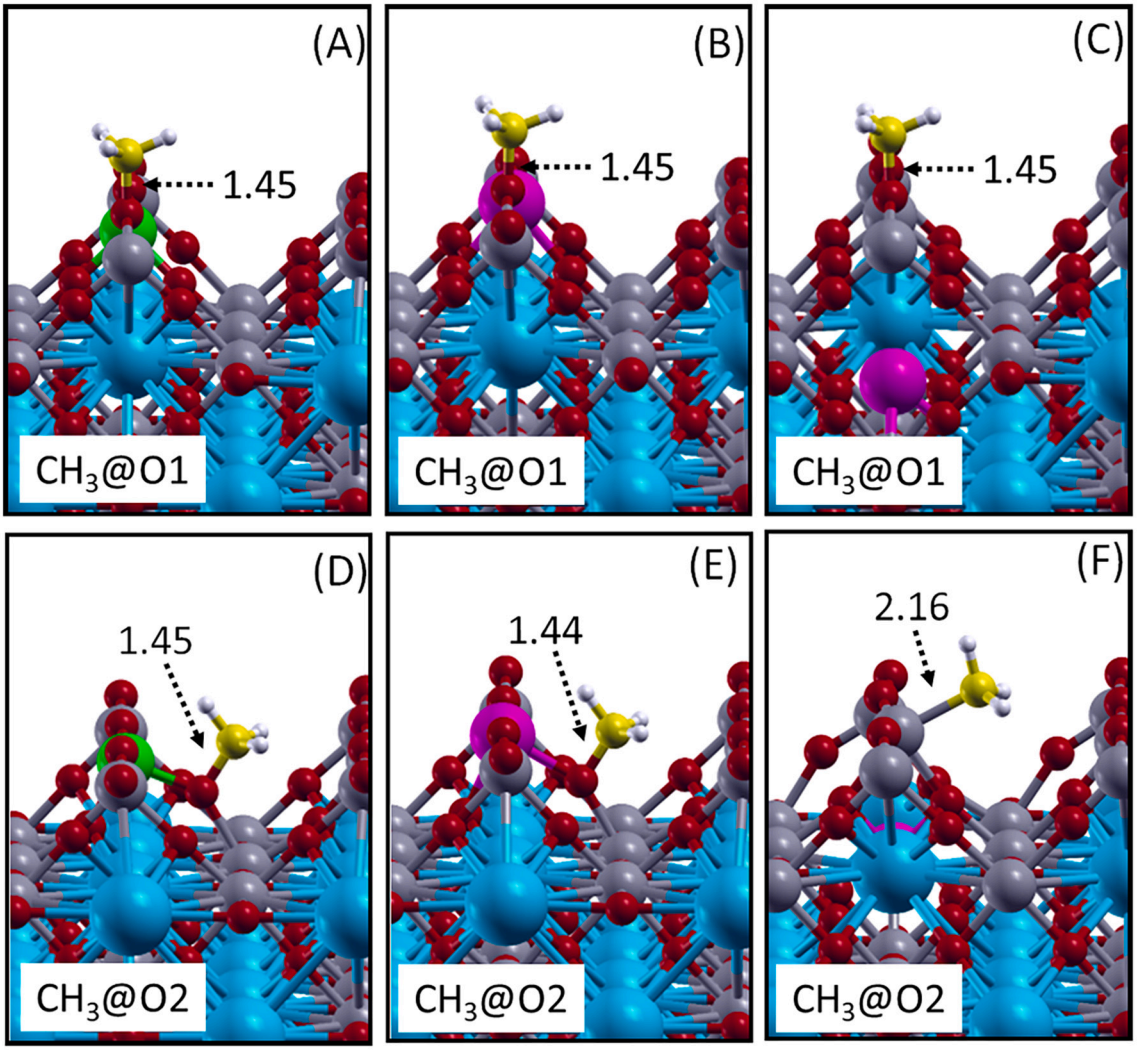

Fig. 3. CH_3 adsorption at O1 (top) and O2 (down) sites for the B- site Al- (A, D), Mg-doped (B, E) and for the A-site Mg-doped (C, D) steps. All distances are reported in Å. Colour code as in Fig. 1. In addition, the yellow, white and magenta spheres are C, H, and Mg atoms, respectively. (For interpretation of the references to colour in this figure legend, the reader is referred to the web version of this article.)

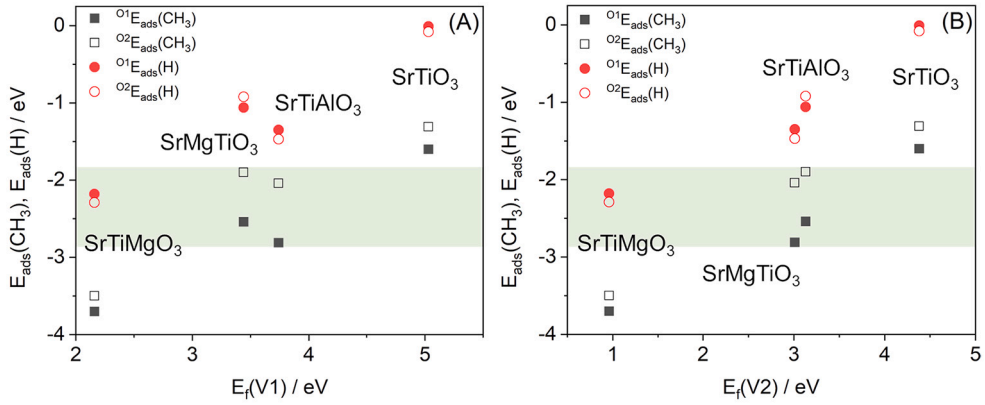

Fig. 4. Linear correlation between (A) $E_f(V1)$ and $E_{ads}(CH_3)/E_{ads}(H)$ and (B) $E_f(V2)$ and $E_{ads}(CH_3)/ E_{ads}(H)$. The filled and empty symbols represent the CH_3/H adsorption at the O1 and O2 adsorption sites, respectively. The $SrTiO_3$, $SrMgTiO_3$, $SrTiAlO_3$, $SrTiMgO_3$ represent the pure, the Mg-doped (A-site), the Al-doped (B-site) and the B-doped (B-site) steps, respectively. All energies are in eV. The green bands are the optimal range for $E_{ads}(CH_3)$ values.

suggests $E_{ads}(CH_3)$ as the optimal parameter to describe the catalytic performance in the OCM, and this conclusion can also be applied to the steps. In fact, in the first instance, one of the crucial stages in the OCM mechanism is the release of the CH_3 into the gas phase, while $E_f(Vx)$ is important to reconstruct the catalyst under the initial conditions. Based on this assumption, each pure and doped step will be evaluated, and the

calculated $E_{ads}(CH_3)$ values will be correlated with the experimental data [20]. The following discussion will be valid for both V1 and V2 sites.

The pure step has a good value for $E_{ads}(CH_3)$, but the too high values of $E_f(Vx)$ for both V1 and V2 invalidate its performance. In fact, experimental data [20] suggest that the pure system is not a good catalyst. The Mg-doped at the A site and the Al-doped at the B site have quite similar values for $E_{ads}(CH_3)$, between 2.5 ± 0.5 eV (see Fig. 4, green bands). The experimental data suggest that these doped systems have good catalytic performance, so it is possible to quantitatively correlate the good catalytic performance with the $E_{ads}(CH_3)$ value. Incidentally, this is the same optimal range already reported in the literature for Ln-doped $SrTiO_3$ [21] and for Al/Mg-doped $SrTiO_3$ surfaces [47].

Finally, the Mg-doped step at the B site has a too high value for $E_{ads}(CH_3)$. This means that CH_3 is so strongly adsorbed that it prevents the release into the gas phase and formation of the desired products. This result seems in contrast with experimental data [20] that found that the Mg-doped at the B site is a good catalyst. The disagreement can be resolved if the Mg-doped surface is also considered. In fact, this surface is easily reduced, so in the presence of the Mg dopant at the B site, the catalyst is mainly a reduced doped surface. The catalytic performance of this Mg-doped reduced surface [47] is in agreement with experimental data [20]. Therefore, the Mg dopant at B-site is not a good catalytic site in the step for the OCM reaction.

Given the linear correlation between $E_{ads}(CH_3)$ / $E_{ads}(H)$, the same considerations could be made when considering $E_{ads}(H)$. The only difference will be the optimal adsorption range. In fact, the pure $SrTiO_3$ step still has $E_f(Vx)$ values that are too high, and $E_{ads}(H)$ for the Mg-doped step at the B-site is also too high. A high value prevents the release of the H atom and the restoration of the catalyst in its initial conditions.

5. Conclusions

The OCM reaction was studied and the mechanism's different stages were investigated using first principles. Catalytic performance depends on three different parameters: oxygen vacancy formation, CH_3 adsorption and C—H dissociation, which are generally accepted in the literature as good descriptors for OCM catalysts. Thus, DFT calculations are used to gain these values for all systems.

To better describe the experimental conditions and correctly reproduce all the experimental data, an ideal model as a flat surface might be inadequate, so a more realistic system with extended structural defect (step), oxygen vacancies and metal (Al and Mg) dopant was considered. Results demonstrated that the inclusion of structural defectivity as the step is crucial to understanding the OCM reaction mechanism.

Outcomes obtained on pure, pure-reduced, doped and doped-reduced systems show that the step has different absorption sites with different behaviour and not all of them are good catalytic sites. For example, too high energy for the CH_3 adsorption implies low selectivity, thus poor catalytic performance. To consider at the same time the influence of selectivity, reducibility and activity, these parameters were correlated and linear trends were found between oxygen vacancy formation and CH_3/H adsorption values for both absorption sites and oxygen vacancy positions. Because of these relationships, only one parameter can be considered and the correlation between experimental performance and calculated values suggests that CH_3 adsorption is the best parameter to consider. Furthermore, this comparison indicates that the optimal range for this parameter is around −2.5 eV. In agreement with experimental data, Al-doped at B-site and Mg-doped at A-site are good catalysts.

A more general comparison between step and surface models under similar conditions shows that step (i) has different adsorption properties than the surface and (ii) is not necessarily the best performing catalytic site. Regarding the first point, the CH_4 adsorption energies are always higher at the step and this suggests that, in the presence of this defect, it becomes the preferred adsorption site. With the CH_3 adsorption values, several adsorption sites are present at the step and their behaviour is different: at the first layer, the adsorption values are higher than at the surface, while the opposite occurs at the second layer. Regarding the second point, the higher step adsorption energies do not always make it a better catalytic site. In fact, as verified for the Mg-doped step at the B-site, too high absorption energy prevents the CH_3 release, making it a poor catalytic site for the OCM reaction. These variations strongly alter the performance of the catalyst and highlight that the results obtained for ideal surfaces are not fully transferable on the step model. Therefore, a study that includes additional defectivities is essential.

CRediT authorship contribution statement

Silvia Carlotto: Conceptualization, Methodology, Validation, Formal analysis, Writing – original draft, Funding acquisition.

Declaration of Competing Interest

The authors declare the following financial interests/personal relationships which may be considered as potential competing interests:

Silvia Carlotto reports financial support was provided by the University of Padua.

Data availability

The data that has been used is confidential.

Acknowledgement

The Computational Chemistry Community (C_3P) of the University of Padova is kindly acknowledged. This work was supported by the University of Padova (Grant P-DISC #CARL-SID17 BIRD2017-UNIPD, Project CHIRoN).

References

[1] A. Galadima, O. Muraza, Revisiting the oxidative coupling of methane to ethylene in the golden period of shale gas: a review, J. Ind. Eng. Chem. 37 (2016) 1–13, https://doi.org/10.1016/J.JIEC.2016.03.027.
[2] J.H. Lunsford, The catalytic oxidative coupling of methane, Angew. Chem. Int. Ed. Eng. 34 (1995) 970–980, https://doi.org/10.1002/anie.199509701.
[3] G.E. Keller, M.M. Bhasin, Synthesis of ethylene via oxidative coupling of methane: I. Determination of active catalysts, J. Catal. 73 (1982) 9–19, https://doi.org/10.1016/0021-9517(82)90075-6.
[4] H. Schwarz, H. Schwarz, Chemistry with methane: concepts rather than recipes, Angew. Chem. Int. Ed. 50 (2011) 10096–10115, https://doi.org/10.1002/ANIE.201006424.
[5] P. Schwach, X. Pan, X. Bao, Direct conversion of methane to value-added chemicals over heterogeneous catalysts: challenges and prospects, Chem. Rev. 117 (2017) 8497–8520, https://doi.org/10.1021/ACS.CHEMREV.6B00715.
[6] A.M. Arinaga, M.C. Ziegelski, T.J. Marks, Alternative oxidants for the catalytic oxidative coupling of methane, Angew. Chem. Int. Ed. 60 (2021) 10502–10515, https://doi.org/10.1002/ANIE.202012862.
[7] J. Liu, J. Yue, M. Lv, F. Wang, Y. Cui, Z. Zhang, G. Xu, From fundamentals to chemical engineering on oxidative coupling of methane for ethylene production: a review, Carbon Res. Conv. 5 (2022) 1–14, https://doi.org/10.1016/J.CRCON.2021.11.001.
[8] C. Karakaya, R.J. Kee, Progress in the direct catalytic conversion of methane to fuels and chemicals, Prog. Energy Combust. Sci. 55 (2016) 60–97, https://doi.org/10.1016/J.PECS.2016.04.003.
[9] B.L. Farrell, V.O. Igenegbai, S. Linic, A viewpoint on direct methane conversion to ethane and ethylene using oxidative coupling on solid catalysts, ACS Catal. 6 (2016) 4340–4346, https://doi.org/10.1021/ACSCATAL.6B01087.
[10] C.A. Ortiz-Bravo, C.A. Chagas, F.S. Toniolo, Oxidative coupling of methane (OCM): an overview of the challenges and opportunities for developing new technologies, J. Nat. Gas Sci. Eng. 96 (2021), 104254, https://doi.org/10.1016/J.JNGSE.2021.104254.
[11] P.R. Murthy, Y. Liu, G. Wu, Y. Diao, C. Shi, Oxidative coupling of methane: perspective for high-value C_2 chemicals, Crystals (Basel). 11 (2021) 1011, https://doi.org/10.3390/CRYST11091011.
[12] Y. Gambo, A.A. Jalil, S. Triwahyono, A.A. Abdulrasheed, Recent advances and future prospect in catalysts for oxidative coupling of methane to ethylene: a review, J. Ind. Eng. Chem. 59 (2018) 218–229, https://doi.org/10.1016/J.JIEC.2017.10.027.

[13] D. Kiani, S. Sourav, J. Baltrusaitis, I.E. Wachs, Oxidative coupling of methane (OCM) by SiO_2-supported tungsten oxide catalysts promoted with Mn and Na, ACS Catal. 9 (2019) 5912–5928, https://doi.org/10.1021/ACSCATAL.9B01585.
[14] G.J. Hutchings, M.S. Scurrell, J.R. Woodhouse, Oxidative coupling of methane using oxide catalysts, Chem. Soc. Rev. 18 (1989) 251–283, https://doi.org/10.1039/CS9891800251.
[15] K. Kwapien, J. Paier, J. Sauer, M. Geske, U. Zavyalova, R. Horn, P. Schwach, A. Trunschke, R. Schlögl, Sites for methane activation on lithium-doped magnesium oxide surfaces, Angew. Chem. Int. Ed. 53 (2014) 8774–8778, https://doi.org/10.1002/anie.201310632.
[16] S. Chrétien, H. Metiu, Acid-base interaction and its role in alkane dissociative chemisorption on oxide surfaces, J. Phys. Chem. C 118 (2014) 27336–27342, https://doi.org/10.1021/jp507207b.
[17] G. Kumar, S.L.J. Lau, M.D. Krcha, M.J. Janik, Correlation of methane activation and oxide catalyst reducibility and its implications for oxidative coupling, ACS Catal. 6 (2016) 1812–1821, https://doi.org/10.1021/acscatal.5b02657.
[18] Z.Q. Wang, D. Wang, X.Q. Gong, Strategies to improve the activity while maintaining the selectivity of oxidative coupling of methane at La_2O_3: a density functional theory study, ACS Catal. 10 (2020) 586–594, https://doi.org/10.1021/acscatal.9b03066.
[19] V. Fung, F. Polo-Garzon, Z. Wu, D. Jiang, Exploring perovskites for methane activation from first principles, Catal. Sci. Technol. 8 (2018) 702–709, https://doi.org/10.1039/C7CY01791J.
[20] D.V. Ivanov, L.A. Isupova, E.Y. Gerasimov, L.S. Dovlitova, T.S. Glazneva, I. P. Prosvirin, Oxidative methane coupling over Mg, Al, Ca, Ba, Pb-promoted $SrTiO_3$ and Sr_2TiO_4: influence of surface composition and microstructure, Appl. Catal. A Gen. 485 (2014) 10–19, https://doi.org/10.1016/j.apcata.2014.07.024.
[21] S. Lim, J.W. Choi, D.J. Suh, K.H. Song, H.C. Ham, J.M. Ha, Combined experimental and density functional theory (DFT) studies on the catalyst design for the oxidative coupling of methane, J. Catal. 375 (2019) 478–492, https://doi.org/10.1016/j.jcat.2019.04.008.
[22] Z. Fakhroueian, F. Farzaneh, N. Afrookhteh, Oxidative coupling of methane catalyzed by Li, Na and Mg doped $BaSrTiO_3$, Fuel. 87 (2008) 2512–2516, https://doi.org/10.1016/J.FUEL.2008.02.010.
[23] Z. Liu, J.P. Ho Li, E. Vovk, Y. Zhu, S. Li, S. Wang, A.P. van Bavel, Y. Yang, Online kinetics study of oxidative coupling of methane over La_2O_3 for methane activation: what is behind the distinguished light-off temperatures? ACS Catal. 8 (2018) 11761–11772, https://doi.org/10.1021/acscatal.8b03102.
[24] P. Huang, Y. Zhao, J. Zhang, Y. Zhu, Y. Sun, Exploiting shape effects of La_2O_3 nanocatalysts for oxidative coupling of methane reaction, Nanoscale. 5 (2013) 10844–10848, https://doi.org/10.1039/c3nr03617k.
[25] Y.H. Hou, W.C. Han, W.S. Xia, H.L. Wan, Structure sensitivity of $La_2O_2CO_3$ catalysts in the oxidative coupling of methane, ACS Catal. 5 (2015) 1663–1674, https://doi.org/10.1021/cs501733r.
[26] J. Xu, Y. Zhang, X. Xu, X. Fang, R. Xi, Y. Liu, R. Zheng, X. Wang, Constructing La2B2O7 (B = Ti, Zr, Ce) compounds with three typical crystalline phases for the oxidative coupling of methane: the effect of phase structures, superoxide anions, and alkalinity on the reactivity, ACS Catal. 9 (2019) 4030–4045, https://doi.org/10.1021/acscatal.9b00022.
[27] M.D. Krcha, A.D. Mayernick, M.J. Janik, Periodic trends of oxygen vacancy formation and C-H bond activation over transition metal-doped CeO_2 (111) surfaces, J. Catal. 293 (2012) 103–115, https://doi.org/10.1016/j.jcat.2012.06.010.
[28] L. Wang, T. Maxisch, G. Ceder, Oxidation energies of transition metal oxides within the GGA+ U framework, Phys. Rev. B 73 (2006), 195107, https://doi.org/10.1103/PhysRevB.73.195107.
[29] S. Carlotto, The role of the dopant and structural defects on the water absorption and on the H_2 formation in the Al, co and cu doped $SrTiO_3$ perovskite steps, Appl. Surf. Sci. 527 (2020), 146850, https://doi.org/10.1016/j.apsusc.2020.146850.
[30] G.S. Foo, F. Polo-Garzon, V. Fung, D.E. Jiang, S.H. Overbury, Z. Wu, Acid-base reactivity of perovskite catalysts probed via conversion of 2-propanol over titanates and zirconates, ACS Catal. 7 (2017) 4423–4434, https://doi.org/10.1021/acscatal.7b00783.
[31] S. Carlotto, M.M. Natile, A. Glisenti, A. Vittadini, Electronic structure of $SrTi_{1-x}M_xO_{3-d}$ (M = Co, Ni, Cu) perovskite-type doped-titanate crystals by DFT and DFT + U calculations, Chem. Phys. Lett. 588 (2013) 102–108, https://doi.org/10.1016/j.cplett.2013.10.020.
[32] S. Carlotto, M.M. Natile, A. Glisenti, A. Vittadini, Adsorption of small molecules at the cobalt-doped $SrTiO_3$(001) surface: a first-principles investigation, Surf. Sci. 633 (2015) 68–76, https://doi.org/10.1016/j.susc.2014.11.025.
[33] S. Carlotto, M.M. Natile, A. Glisenti, J.F. Paul, D. Blanck, A. Vittadini, Energetics of CO oxidation on lanthanide-free perovskite systems: the case of Co-doped $SrTiO_3$, Phys. Chem. Chem. Phys. 18 (2016) 33282–33286, https://doi.org/10.1039/c6cp03994d.
[34] S. Carlotto, M.M. Natile, A. Glisenti, A. Vittadini, Adsorption of CO and formation of carbonates at steps of pure and Co-doped $SrTiO_3$ surfaces by DFT calculations, Appl. Surf. Sci. 364 (2016) 522–527, https://doi.org/10.1016/j.apsusc.2015.12.194.
[35] L. Bai, F. Polo-Garzon, Z. Bao, S. Luo, B.M. Moskowitz, H. Tian, Z. Wu, Impact of surface composition of $SrTiO_3$ catalysts for oxidative coupling of methane, ChemCatChem. 11 (2019) 2107–2117, https://doi.org/10.1002/cctc.201900159.
[36] P. Giannozzi, S. Baroni, N. Bonini, M. Calandra, R. Car, C. Cavazzoni, D. Ceresoli, G.L. Chiarotti, M. Cococcioni, I. Dabo, A. Dal Corso, S. de Gironcoli, S. Fabris, G. Fratesi, R. Gebauer, U. Gerstmann, C. Gougoussis, A. Kokalj, M. Lazzeri, L. Martin-Samos, N. Marzari, F. Mauri, R. Mazzarello, S. Paolini, A. Pasquarello, L. Paulatto, C. Sbraccia, S. Scandolo, G. Sclauzero, A.P. Seitsonen, A. Smogunov, P. Umari, R.M. Wentzcovitch, QUANTUM ESPRESSO: a modular and open-source software project for quantum simulations of materials, J. Phys. Condens. Matter 21 (2009), 395502, https://doi.org/10.1088/0953-8984/21/39/395502.
[37] P. Giannozzi, O. Andreussi, T. Brumme, O. Bunau, M. Buongiorno Nardelli, M. Calandra, R. Car, C. Cavazzoni, D. Ceresoli, M. Cococcioni, N. Colonna, I. Carnimeo, A. Dal Corso, S. de Gironcoli, P. Delugas, R.A. Distasio, A. Ferretti, A. Floris, G. Fratesi, G. Fugallo, R. Gebauer, U. Gerstmann, F. Giustino, T. Gorni, J. Jia, M. Kawamura, H.Y. Ko, A. Kokalj, E. Küçükbenli, M. Lazzeri, M. Marsili, N. Marzari, F. Mauri, N.L. Nguyen, H.V. Nguyen, A. Otero-De-La-Roza, L. Paulatto, S. Poncé, D. Rocca, R. Sabatini, B. Santra, M. Schlipf, A.P. Seitsonen, A. Smogunov, I. Timrov, T. Thonhauser, P. Umari, N. Vast, X. Wu, S. Baroni, Advanced capabilities for materials modelling with quantum ESPRESSO, J. Phys. Condens. Matter 29 (2017), 465901, https://doi.org/10.1088/1361-648X/AA8F79.
[38] S. Carlotto, A. Vittadini, M. Casarin, DFT modelling of the CO-NO redox reaction at cu-doped $SrTiO_3$(1 0 0) stepped surface: CO oxidation at lattice O ions, Inorg. Chim. Acta 511 (2020), 119810, https://doi.org/10.1016/j.ica.2020.119810.
[39] S. Carlotto, A. Vittadini, M. Casarin, DFT modelling of the NO reduction process at the cu-doped $SrTiO_3$(1 0 0) stepped surface, Inorg. Chim. Acta 511 (2020), 119813, https://doi.org/10.1016/j.ica.2020.119813.
[40] J.P. Perdew, K. Burke, M. Ernzerhof, Generalized gradient approximation made simple, Phys. Rev. Lett. 77 (1996) 3865–3868, https://doi.org/10.1103/PhysRevLett.77.3865.
[41] D. Vanderbilt, Soft self-consistent pseudopotentials in a generalized eigenvalue formalism, Phys. Rev. B 41 (1990) 7892–7895, https://doi.org/10.1103/PhysRevB.41.7892.
[42] Y.-L. Lee, J. Kleis, J. Rossmeisl, D. Morgan, Ab initio energetics of $LaBO_3$ (001) (B = Mn, Fe, Co, and Ni) for solid oxide fuel cell cathodes, Phys. Rev. B 80 (2009), 224101, https://doi.org/10.1103/PhysRevB.80.224101.
[43] Z. Stansch, L. Mleczko, M. Baerns, Comprehensive kinetics of oxidative coupling of methane over the La_2O_3/CaO catalyst, Ind. Eng. Chem. Res. 36 (1997) 2568–2579, https://doi.org/10.1021/IE960562K.
[44] G.E. Keller, M.M. Bhasin, Synthesis of ethylene via oxidative coupling of methane: I. Determination of active catalysts, J. Catal. 73 (1982) 9–19, https://doi.org/10.1016/0021-9517(82)90075-6.
[45] C. Karakaya, H. Zhu, B. Zohour, S. Senkan, R.J. Kee, Detailed reaction mechanisms for the oxidative coupling of methane over La_2O_3/CeO_2 nanofiber fabric catalysts, ChemCatChem. 9 (2017) 4538–4551, https://doi.org/10.1002/CCTC.201701172.
[46] V.I. Lomonosov, M.Y. Sinev, Oxidative coupling of methane: mechanism and kinetics, Kinet. Catal. 57 (2016) 652–684, https://doi.org/10.1134/S0023158416050128.
[47] S. Carlotto, The catalytic performance of pure, doped, and reduced-doped $SrTiO_3$ perovskite surfaces for oxidative coupling of methane, Appl. Surf. Sci. 602 (2022), 154376, https://doi.org/10.1016/J.APSUSC.2022.154376.